Published in final edited form as:
Aviat Space Environ Med. 2011 April ; 82(4): 424–433.

Static and Dynamic Autonomic Response with Increasing Nausea Perception

Lauren T LaCount, BS[1], **Riccardo Barbieri, PhD**[2,3], **Kyungmo Park, PhD**[4], **Jieun Kim, PhD**[1], **Emery N Brown, MD PhD**[2,3], **Braden Kuo, MD**[5], and **Vitaly Napadow, PhD**[1,6,*]

[1]Martinos Center for Biomedical Imaging, Department of Radiology, Massachusetts General Hospital, Charlestown, MA, USA

[2]Department of Anesthesia and Critical Care, Massachusetts General Hospital, Boston, MA, USA

[3]Department of Brain and Cognitive Science, Massachusetts Institute of Technology, Cambridge, MA, USA

[4]Department of Biomedical Engineering, Kyunghee University, Yongin, Republic of Korea

[5]Gastroenterology Unit, Massachusetts General Hospital, Harvard Medical School, Boston, MA, USA

[6]Department of Radiology, Logan College of Chiropractic, Chesterfield, MO, USA

Abstract

Background—Nausea is a commonly occurring symptom typified by epigastric discomfort with urge to vomit. The relationship between autonomic nervous system (ANS) outflow and increasing nausea perception is not fully understood.

Methods—Our study employed a nauseogenic visual stimulus (horizontally translating stripes) while 17 female subjects freely rated transitions in nausea level and autonomic outflow was measured (heart rate, HR, heart rate variability, HRV, skin conductance response, SCR, respiratory rate). We also adopted a recent approach to continuous high frequency (HF) HRV estimation to evaluate dynamic cardiovagal modulation.

Results—HR increased from baseline for all increasing nausea transitions, especially transition to strong nausea (15.0±11.4 bpm), but decreased (−6.6±4.6 bpm) once the visual stimulus ceased. SCR also increased for all increasing nausea transitions, especially transition to strong nausea (1.76±1.68 μS), but continued to increase (0.52 ± 0.65 μS) once visual stimulation ceased. LF/HF HRV increased following transition to moderate (1.54±2.11 a.u.) and strong (2.57±3.49 a.u.) nausea, suggesting a sympathetic shift in sympathovagal balance. However, dynamic HF HRV suggested that bursts of cardiovagal modulation precede transitions to higher nausea, perhaps influencing subjects to rate higher levels of nausea. No significant change in respiration rate was found.

Conclusions—Our results suggest that increasing nausea perception is associated with both increased sympathetic and decreased parasympathetic ANS modulation. These findings corroborate past ANS studies of nausea, applying percept-linked analyses and dynamic estimation of cardiovagal modulation in response to nausea.

[*]**Corresponding Address:** Vitaly Napadow, PhD Martinos Center for Biomedical Imaging 149 Thirteenth St. #2301 Charlestown, MA 02129 617-724-3402 vitaly@nmr.mgh.harvard.edu.

Keywords

motion sickness; heart rate variability; skin conductance response; galvanic skin response; vestibular

Introduction

Nausea is a commonly occurring symptom typified by epigastric discomfort with the urge to vomit. It can arise from a variety of causes including as a side effect of pharmacotherapy and general anesthesia, as a side effect of fluctuating hormone levels during pregnancy, and as a consequence of visual / vestibular sensory discordance. This latter cause, termed motion sickness, typifies the root of the word “nausea” (derived from “naus” or “ship” in Greek), and has been commonly adopted in experimental settings to study physiological responses to nausea [24].

Motion sickness is a conglomeration of individual symptoms, which can be grouped by factor analysis [19]. One factor is specifically related to nausea and includes the following symptoms: stomach awareness, burping, increased salivation, sweating, and nausea. However, other factors include oculomotor (e.g. eye strain, blurred vision), and disorientation (e.g. dizziness) symptoms, which are all concomitant with nausea during motion sickness. Severity or even occurrence of motion sickness varies appreciably among individuals, and motion sickness symptoms and susceptibility have a complex relationship with ethnicity and gender. For instance, individuals of Asian descent tend to be more susceptible to motion sickness than Caucasian individuals [22, 24], and responses to motion sickness susceptibility questionnaires have been found to differ between males and females [22].

The underlying mechanism of motion sickness is postulated to be a conflict between the visual and vestibular systems, but can also occur due to conflict within the vestibular [34] and visual [20] systems themselves. Hence experimental induction of motion sickness has appropriated rotating chairs [11, 13, 16, 18, 30, 37], virtual reality or simulator systems [21, 28]; or optokinetic drums [8], in which the subject remains stationary and a striped drum rotates around their head. Ultimately, motion sickness is known to be strongly influenced by the autonomic nervous system (ANS) [17, 31], as well as vestibular [17], cognitive [24], and neuroendocrine systems [17].

ANS response to nausea spans multiple end-organs and includes both sympathetic and parasympathetic outflow. Prior studies have measured a variety of autonomic physiological variables and have generally found that motion sickness increases both heart rate [10, 21, 28, 37] and skin conductance [10, 18, 21], a measure of sympathetic output to sudomotor glands in the skin [17]. More precise cardio-autonomic modulation has been estimated by measures of heart rate variability (HRV). With this analysis approach, spectral analysis assesses sympathovagal modulation by measuring the magnitude of a high-frequency (influenced by cardiovagal outflow) and low-frequency (both sympathetic and parasympathetic) peak in the heart rate power spectrum [26]. High-frequency (“HF”) HRV has been found to decrease during motion sickness [13] in one study, increase during another [21], and remain unchanged in a third [30]. This inconsistency may have been due to variability in stimulus intensity (stemming from the form of motion sickness stimulus used [20] – i.e. visual only [21] versus actual physical rotation [13, 30]) as well as measurement and analysis techniques [13, 21, 30].

In this study, we aimed to address inconsistencies in past studies as well as apply recent adaptive point-process algorithms for estimating dynamic HRV response to illusory motion induced nausea. We applied an experimental design wherein a visual display of translating stripes encompasses the entire field of view for supine individuals previously deemed susceptible to motion sickness. Skin conductance, electrocardiography, and respiration were all monitored in order to assess various ANS response metrics in conjunction with subjective naturalistic report of worsening nausea. We hypothesized that increasing nausea would elicit increasing sympathetic modulation, while dynamic trends in HF HRV would demonstrate characteristic fluctuations of parasympathetic (cardiovagal) modulation both prior and following subjective transitions to increasing nausea.

Methods

Subjects

Participants included female, right-handed (Edinburgh Inventory [33]) subjects with a mean age of 28.4 years (s.d.=8.5years) and increased susceptibility to motion sickness, as indicated by a score greater than 60 on the Motion Sickness Susceptibility Questionnaire [15]. A MSSQ level of 60 was chosen because it represented a visible inflection point in the graph provided by the study developing this instrument. Thus, subjects with MSSQ scores higher than 60 reliably reached moderate nausea perception and did so faster than those with lower scores [15]. Subjects were instructed to abstain from food and water for 12 hours, and from cigarettes and alcohol for 24 hours, prior to the experiment. This was deemed necessary for safety reasons, as subjects would be stimulated to the verge of vomiting. All experiments took place between 7 a.m. and 12 p.m. at the Martinos Center for Biomedical Imaging in Boston, MA. Informed consent was obtained from all participants, and the protocol was approved by the Human Research Committee of Massachusetts General Hospital.

30 motion sickness prone subjects underwent a training session (see below), with 21 experiencing high enough nausea that they were asked to continue on to the next experimental session, which was performed inside an MRI scanner. Of the 21 subjects who completed the experimental session, three were not included in our analyses because their maximum nausea rating was a “2” (“moderate” nausea, see below). This was done to limit heterogeneity in subjects, such that all subjects included in the analysis reached at least a “strong,” if not “severe” level of nausea. Another subject was not included because her preexperiment (*baseline*) nausea level started at a “2,” while all other subjects began at “0.” Thus, 17 subjects were ultimately included in the analysis. Due to MRI scanner noise, the ECG could not be annotated for one subject, who was thus excluded from heart rate (HR) and HRV analyses, while three other subjects had poor respiratory data quality and were excluded from those analyses.

Procedure

The study was divided into two sessions. During the first (training) session, subjects were familiarized with the experimental setup and nauseogenic stimulus. If subjects attained a sufficiently high level of nausea and if they chose to remain in the study, they returned (at least 12 days later) to a second experimental session. The physiological data presented here were collected as part of this second, more controlled, experimental session that also included functional MRI data acquisition. FMRI data will be presented in a future publication as they are outside the scope of this ANS-focused analysis.

Subjects were placed, supine, in a 1.5T Siemens Avanto MRI Scanner (Siemens Medical Systems, Erlangen, Germany). A specialized 23-channel head coil constructed at the

Martinos Center for Biomedical Imaging [38] was used to allow for unimpeded visual stimulation. A concave screen was positioned 10cm in front of their eyes, onto which visual stimuli were projected, from behind. The head of the subject was immobilized in the MRI head coil, with cushions on either side, thereby insuring no head tilt maneuvers (Figure 1a), which are known to strongly influence visual stimulus induced motion sickness via pseudo-Coriolis effects [6]. Importantly, the concave screen comprised the entire field-of-view (150°) of the subject. The visual stimulus procedure for both sessions was divided into three different (but contiguous) periods (Figure 1b). The first and last periods were each five minutes in length, during which subjects were asked to lie still and stare directly ahead at a cross-hair projected onto the center of the screen. Between these two periods, subjects were presented with a nauseogenic visual stimulus of black/white stripes (black stripes 1.2cm, 6.9° viewing angle; white stripes 1.85cm, 10.6° viewing angle) translating left-to-right at an apparent speed of 62.5°/sec. This left-to-right horizontal translation induces a linear vection sensation wherein subjects experience a false sensation of translating to the left [20, 24]. Similar full field-of-view vection stimuli in supine subjects have successfully been used in the past [9]. The maximum duration of our nauseogenic stimulus was 20 minutes, but was shortened in some subjects based on these subjects reaching a predetermined maximum level of discomfort (see below). Subjects were instructed to maintain a constant, natural, respiratory rate throughout the experiment to improve HRV interpretability [4, 26] and to prevent self-inhibition of increasing nausea [1, 12]. Subjects were also asked to keep their eyes open and just let the nausea sensation evolve, knowing that a rating of severe nausea will terminate the stimulus. These instructions were described before and after the training session, in order to give subjects feedback and practice in limiting self-inhibition. Instructions were again repeated just prior to the experimental session.

Subjects were instructed to rate their level of nausea using an intensity scale of “0” to “4.” These ratings were practiced during the training session, to better familiarize subjects with rating nausea intensity. Subjects were instructed that a rating of “4” indicated “severe” nausea, where subjects felt they were on the verge of vomiting from their past experience. A rating of “3” indicated “strong” nausea, a rating of “2” “moderate” nausea, a rating of “1” indicated “mild” nausea, and a rating of “0” indicated no nausea. Subjects knew that once they rated “4” for severe nausea, the stimulus would be terminated. During the experimental session, subjects were trained to use a 5-button button box to freely (not cued) rate their overall nausea level ranging from “0” to “4”.

Following the experiment, subjects completed the Simulator Sickness Questionnaire (SSQ) [19], to report the severity of different motion sickness symptoms at each global (0–4) nausea level. As previously mentioned, motion sickness symptoms presented in the SSQ can be grouped into three factors: (1) nausea, (2) oculomotor, and (3) disorientation [19]. A SSQ factor score was thus calculated for each global nausea level for each subject. We then used repeated-measures ANOVA to test for significant differences in factor score amongst these global nausea levels, followed by post hoc paired *t*-tests to determine which global levels were significantly different from one another for each SSQ factor.

Equipment and Single Subject Analysis

All physiological signals were collected at 400 Hz using Chart Data Acquisition Software (ADInstruments, Colorado Springs, CO) on a laptop equipped with a 16 Channel Powerlab DAQ System (ADInstruments, Colorado Springs, CO). Physiological metrics were calculated within discrete windows of time (see below) using in-house developed tools (Matlab v. 7.1, The MathWorks, Inc., Natick, MA).

Skin Conductance Response (SCR)—During the experiment, skin conductance level (SCL) was measured with Ag/AgCl finger electrodes (MLT117F, ADInstruments, Colorado Springs, CO) attached to the palmar aspect of the second and fourth fingers of the non-dominant left hand. A 10 Hz low pass filter was applied to the skin conductance signal. Mean SCL was calculated for discrete windows and compared to baseline according to the analysis procedures below.

Heart Rate (HR)—An MRI-compatible Patient Monitor (Model 3150, InVivo Research, Inc., Orlando, FL) was used to collect subjects' electrocardiogram (ECG) signal through MRI-compatible electrodes (VerMed, Bellows Falls, VT) on the chest. Due to the existence of gradient switching artifact from the MRI scanner, HR and R-R interval obtained from ECG data were first annotated using automated methods (WaveForm DataBase Software Package; [14]) followed by manual adjustments (Matlab v. 7.1, The MathWorks, Inc., Natick, MA) to assure correct QRS peak detection. Within each window of interest, the average heart rate was calculated. Due to MRI scanner noise, the ECG could not be annotated for one subject, who was thus excluded from HR and HRV analyses.

Heart Rate Variability (HRV)—HRV was calculated from the same ECG signal used to calculate heart rate above. HRV for discrete time windows was calculated from the power spectral density of heart rate (resampled at 4Hz from the inverted RR interval time series) using in-house tools (Matlab v. 7.1, The MathWorks, Inc., Natick, MA). Calculations were performed for 4 min windows. The low-frequency power (LF) within each window was computed by taking the integral of the power spectrum between 0.04 and 0.15 Hz, while the high-frequency power (HF) was computed as the integral between 0.15 and 0.4 Hz. Normalized low-frequency power (LFu) and normalized high-frequency power (HFu) were evaluated by dividing LF and HF respectively by the integral of the power spectrum above 0.04. The ratio of LF to HF was also calculated following standard recommendations [26].

In addition, a novel adaptive recursive algorithm was applied to the R–R series to compute instantaneous estimates of heart rate and HRV from electrocardiogram recordings of R-wave events – i.e. “dynamic HRV”. This approach is based on the point process methods already used to develop both local likelihood [2] and adaptive [3] heart rate estimation algorithms. This novel assessment of HRV has also been applied successfully in conjunction with fMRI recordings to characterize the brain correlates of cardiovagal modulation [32]. The stochastic structure in R–R intervals is modeled as an inverse Gaussian renewal process. The inverse Gaussian probability density is derived directly from an elementary, physiologically-based integrate-and-fire model [2, 3].

We assume that given any *R*-wave event u_n, the waiting time until the next *R*-wave event, or equivalently, the length of the next *R-R* interval, obeys an inverse Gaussian probability density $f(t|u_n,\theta)$ where $t > u_n$. The model is defined, at any time t, as

$$f(t|H_{u_k},\theta)=\left[\frac{\theta_{p+1}}{2\pi(t-u_k)^3}\right]^{\frac{1}{2}}\exp\left\{-\frac{1}{2}\frac{\theta_{p+1}[t-u_k-\mu(H_{u_k},\theta)]^2}{\mu(H_{u_k},\theta)^2(t-u_k)}\right\} \quad (1)$$

where $H_{u_k}=\{u_k, w_k, w_{k-1}, \ldots, w_{k-p+1}\}$, $w_k = u_k - u_{k-1}$ is the k^{th}*R-R* interval, $\mu(H_{u_k},\theta)=\theta_0+\sum_{j=1}^{p}\theta_j w_{k-j+1} > 0$ is the mean, $\theta_{p+1} > 0$ is the scale parameter, and $\theta = (\theta_0, \theta_1, \ldots, \theta_{p+1})$.

The model also represents the dependence of the R-R interval length on the recent history of parasympathetic and sympathetic inputs to the SA node by modeling the mean as a linear function of the last p R-R intervals. This set of p coefficients allows for decomposition of the spectral power (HRV) into the classic spectral components noted above: LF and HF [27].

The point process recursive algorithm is able to estimate the dynamics of the model parameters, and consequently the time-varying behavior of each spectral index, at any time resolution. This statistical model for deriving the HRV timeseries has been cross-validated with standard time-frequency domain approaches for HRV analysis [2]. The dynamic response for the point process method was found to provide a significant improvement in tracking fast dynamic changes when compared to the more conventional RLS algorithm [3]. A fixed order p=8 was chosen for the current analysis. Indices were updated every 10 ms and then resampled at 2 Hz.

For all subjects, Dynamic (point-process) HF HRV data were analyzed over 5 different 90-second temporal windows – from 30 seconds before a “transition” to 60 seconds after that transition. For each subject, these “transitions” included the onset of the linear vection stimulus, “START;” rating increase from a level of 0 to a level of 1, “0-to-1;” increase to a rating level of 2, “1-to-2;” increase to a rating level of 3, “2-to-3;” and termination of the linear vection stimulus, “END”. For consistency, the END window was only analyzed for subjects (n=12) whose stimulus was terminated after they rated 4 (some subjects, n=5, only reached a level 3). In order to average across subjects, these data were variance normalized by subtracting the mean and dividing by the standard deviation.

Respiration—Respiration rate was calculated using the end tidal CO_2 ($etCO_2$) level collected via nasal cannula (Salter Labs, Arvin, CA) and the MRI-compatible Patient Monitor noted above. Average respiratory rate was estimated as the frequency of peak power of the discrete Fourier transform of the $etCO_2$ signal within each window of interest. Three subjects had poor respiratory data quality due to equipment failure and were excluded from analyses.

Group Data Analysis and Statistics

As subjects freely rated evolving nausea, analysis of SCR, HR, static HRV, and respiratory rate was performed through both a *stimulus*- as well as *percept-based* approaches (Figure 1c,d). The former was necessary to capture ANS response following vection stimulus termination, while the latter was necessary as different subjects rated nausea level transitions at different times during the experiment. For both approaches, the four-minute period immediately preceding the beginning of the nausea stimulus (“I” or “baseline”) was used as a comparator baseline.

In the stimulus-based approach, which did not explicitly respect subject ratings, four minute windows were taken immediately after the onset of the stimulus (“II”) to reflect initial response, during the last four minutes of the stimulus (“III”) when the subjects were the most nauseous, and during the four minutes immediately following the end of the stimulus (“IV”) as the subjects recovered. A window length of four minutes was chosen to balance potential non-stationarity within the window with the need for adequate data vector size for HRV analyses.

In the percept-based approach, one-minute windows beginning at nausea level transitions (e.g. “1” to “2,” or “2” to “3”) were compared to the baseline level and to one another in order to determine ANS response to increasing perception of nausea symptoms. If subjects had more than one increasing nausea level transition (due to nausea level fluctuation), only the first such transition was used in order to limit heterogeneity.

For both analysis methods, physiological measures were compared with each other and with baseline in two steps. We first used a repeated measures analysis of variance (ANOVA) to test for significant differences among the windows of interest, followed by post-hoc paired *t*-tests to determine which windows were significantly different from one another. As there were multiple post-hoc tests covering multiple windows of interest, a Bonferroni correction was applied to correct for multiple comparisons. Significance was set at $p=0.05$, with $0.1>p>0.05$ considered trending values (SPSS for Windows v. 10.0.7, SPSS, Inc., Chicago, IL).

An example of evolving nausea rating, SCL, HR, point process HF power, and respiratory rate from one subject over the course of the experiment are presented in a Supplementary Figure.

Results

Of the 17 subjects enrolled in this analysis (rating at least a “3” out of “4”), 12 subjects experienced nausea rated as “4,” severe. The average duration of linear vection stimulus for those 12 subjects whose maximum nausea rating was “4” (and therefore terminated prior to the maximum 20 minutes) was 9.1 ± 4.5 minutes (mean ± s.d.). For other intermediate nausea level transitions for all 17 subjects, the average duration until subjects reached the 0-to-1 transition was 1.9 ± 2.1 minutes, the 1-to-2 transition was 3.8 ± 2.3 min, and the 2-to-3 transition was 6.9 ± 4.3 min. Nine (9) of the 17 subjects monotonically increased their nausea ratings without any decreasing nausea level transitions. Eight (8) subjects exhibited at least one decreasing level transition at some point during the experiment, which is not uncommon in linear vection studies where nausea sensation is known to fluctuate. This “drop-off” may have been due to spontaneous change in gaze focus and/or attention processes.

Of the 12 subjects who reached a global nausea level of 4, nine (9) subjects completed the SSQ. An initial repeated measures ANOVA indicated that there were differences in SSQ nausea factor intensity between the different global (0–4) nausea levels for the nausea specific factor ($F(3,24)=119.4$, $p<0.001$), oculomotor factor ($F(1.3,10.4)=37.1$, $p<0.001$, using Greenhouse-Geisser correction for Maulchy's W of 0.01 indicating non-sphericity), and disorientation factor ($F(3,24)=86.7$, $p<0.001$). Post hoc testing demonstrated that all three symptom factors (nausea, oculomotor and disorientation) increased in severity with increasing global nausea level ratings ($p<0.01$ for all comparisons).

For the stimulus-based analysis, four 4-minute temporal windows (immediately before and after both the onset and termination of the nauseogenic stimulus: “I,” “II,” “III,” and “IV”) were compared (Figure 2A), revealing increases in SCR, HR, and LF/HF HRV over the course of the experiment. An initial repeated measures ANOVA indicated that there were within-subject differences among stimulus-based windows for average SCR ($F(1.3,20.8)=15.7$, $p<0.001$, using Greenhouse-Geisser correction for Maulchy's W of 0.04) (Figure 2B), HR ($F(3,45)=16.7$, $p<0.001$) (Figure 2C), and the ratio of LF to HF ($F(3,45)=3.5$, $p=0.02$) (Figure 2G) but not for respiratory rate ($F(3,39)=0.6$, $p=0.6$), normalized HF ($F(3,45)=1.9$, $p=0.1$), and normalized LF ($F(3,45)=1.9$, $p=1$) (Figures 2D, 2E, and 2F, **respectively**).

For the post hoc analyses, average SCL significantly increased over baseline for windows II, III and IV (II: $\Delta = 0.68 \pm 0.98$ μS (mean±s.d.), $p<0.05$; III: 1.94 ± 1.65 μS, $p<0.001$; IV: 2.46 ± 2.11 μS, $p<0.001$) (Figure 2B, Table 1). SCL also increased over the course of the experiment (II to III: $\Delta = 1.26 \pm 1.71$ μS, $p<0.05$; II to IV: $\Delta = 1.78 \pm 2.25$ μS, $p<0.05$; III to IV: $\Delta = 0.52 \pm 0.65$ μS, $p<0.05$) (Figure 2B).

HR increased significantly over baseline for window II (Δ = 7.4±8.2 beats per minute (bpm), p<0.01); III (Δ = 12.0±7.0 bpm, p<0.001) and had a trending increase over baseline for window IV (Δ = 5.4±8.1 bpm, p=0.05) (Figure 2C, Table 2). Average HR increased significantly from II to III (Δ = 4.6±6.1 bpm, p<0.05), but decreased significantly from III to IV (Δ = -6.6±4.6 bpm, p<0.001) after the stimulus terminated (Figure 2C).

In regard to HRV, the ratio of LF to HF trended upward (Δ = 0.92±1.52 a.u., p=0.08) between windows II and III (Figure 2G). No other significant differences or trends were found.

For the percept-based analysis approach, we compared 1-minute temporal windows beginning just after state transition with baseline values (Figure 3A). Overall, we found increases in SCR, HR, normalized LF, and LF/HF, and a decrease in normalized HF. An initial repeated measures ANOVA indicated significant differences among percept-based analysis windows for SCR ($F(3,48)=13.7$, $p<0.001$) (Figure 3B), HR ($F(3,45)=18.4$, $p<0.001$) (Figure 3C), normalized HF ($F(3,45)=3.6$, $p=0.02$) (Figure 3E), normalized LF ($F(3,45)=4.0$, $p=0.01$) (Figure 3F), and the ratio of LF to HF ($F(3,45)=5.7$, $p<0.01$) (Figure 3G), but not respiratory rate ($F(3,39)=0.5$, $p=0.7$) (Figure 3D).

In the post hoc analyses, SCR increased for 0-to-1 (Δ = 0.99±1.26 μS, p<0.05), for 1-to-2 (Δ = 1.32±1.31 μS, p<0.01), and for 2-to-3 (Δ = 1.76±1.68 μS, p<0.01) (Figure 3B, Table 1). SCR also significantly increased with increasing nausea level (from 0-to-1 to 2-to-3: Δ = 0.77±1.13 μS, p<0.05, and from 1-to-2 to 2-to-3: Δ = 0.44±0.67 μS, p<0.05) (Figure 3B).

HR significantly increased in all windows of interest (0-to-1: Δ = 8.4±7.0 bpm, p<0.001; 1-to-2: Δ = 12.7±10.4 bpm, p<0.001; 2-to-3: Δ = 15.0±11.4 bpm, p<0.001) (Figure 3C, Table 2). HR also significantly increased between 0-to-1 and 2-to-3 (Δ = 6.6±8.9 bpm, p<0.05) (Figure 3C).

In regard to HRV, normalized HF significantly decreased from baseline following the 2-to-3 rating transition window (Δ = −0.11±0.13 a.u., p<0.05) (Figure 3E), while normalized LF significantly increased following the 2-to-3 window (Δ = 0.13±0.16 a.u., p<0.05) (Figure 3F). The LF/HF ratio also significantly increased over baseline following both the 1-to-2 transition (Δ = 1.54±2.11 a.u., p<0.05) and the 2-to-3 transition (Δ = 2.57±3.49 a.u., p<0.05) (Figure 3G, Table 3).

Point-process HF HRV data were analyzed for five 90-second temporal windows (START, 0-to-1, 1-to-2, 2-to-3, and END), averaged over all subjects (Figure 4). For these group data, the “START” window demonstrated increasing HF, peaking 10 to 20 seconds after stimulus onset, with gradual decrease thereafter. Conversely, the “END” window demonstrated gradual increase in HF following stimulus cessation. The 0-to-1, 1-to-2, and 2–3 windows demonstrated gradual decrease in HF by 30 seconds after transition in nausea level, but interestingly, phasic bursts of HF *increase* were also seen 10 to 20 seconds before subjects rated a change in nausea level.

Discussion

The autonomic outflow related to increasing nausea sensation following motion sickness is not fully understood. Our study employed a nauseogenic visual stimulus (horizontally translating stripes) while subjects freely rated transitions in their level of nausea and while we measured autonomic outflow to multiple end-organs (heart, skin). Our design allowed us to relate ANS modulation with subject-specific nausea perception. Moreover, we adopted a recent [2, 3] approach to continuous HRV estimation in order to evaluate dynamic cardiovagal response to increasing nausea perception. We found that nausea correlates with

increased heart rate and skin conductance and has a more complex effect on measures of heart rate variability consistent with decreased cardiovagal modulation and a sympathetic shift in sympathovagal balance. Interestingly, our dynamic HRV measures demonstrated that bursts of cardiovagal modulation may accompany transitions in nausea percept level. Specifically, these bursts anticipate and may even play a role in promoting subjects to rate higher levels of nausea. Our findings both corroborate several past autonomic studies of nausea, as well as apply, for the first time, dynamic tracking of cardiovagal modulation in response to increasing nausea perception.

Our study investigated nausea-related changes in HRV with both window-based (assumed stationary in time) and dynamic methods. In the first approach, which considered HF normalized, LF normalized, and LF/ HF over the same intervals used for other physiological variables (HR, SCL), we found an overall decrease in HF normalized. This was coincident with an overall increase in LF normalized and, consequentially, an increase in LF to HF ratio during the presentation of the nauseogenic stimulus. These results are consistent with the tilting of sympathovagal balance away from cardiovagal modulation in response to increasing nausea intensity. We instructed subjects to not significantly alter their respiratory rate to self-inhibit nausea, and the lack of significant change in respiratory rate during the nauseogenic stimulation bolsters the interpretability of these HRV results [4, 26].

Previous studies [13, 21, 30] also examined the effect of motion sickness-induced nausea on measures of HRV. However, these studies did not yield consistent findings. These inconsistencies may stem from differences in stimulus form (visual only versus both physical and visual) and intensity, differences in subject posture, or from methodological approaches to calculate HRV. Different nauseogenic stimuli (e.g. translating stripes versus a rotating chairs) may lead to different intensities of motion sickness and induce different autonomic response patterns [6, 10]. In previous studies exploring HRV, only Kim et al. used visual stimulation without physical rotations or tilt, and found, contrary to our results of decreased HF, an increase in a spectral metric analogous to HF HRV [21]. However, the stimulus used by Kim et al. (naturalistic virtual reality game immersion) was likely much less nauseogenic than our stimulus (horizontally translating stripes), as we stimulated all subjects to “strong” nausea and most subjects all the way to “severe” nausea, on the verge of vomiting. In contrast, the study by Kim et al. included data from all subjects, only 79% of whom experienced *any* motion sickness [21]. Thus, our stimulus was likely stronger and induced a more cardio-sympathetic tilt in sympathovagal balance, with decreased cardiovagal modulation. In addition, posture (e.g. standing versus seated versus supine) is also known to strongly influence HRV [26]. Specifically, in previous studies, subjects were seated, not lying supine as in our study. Finally, HRV is known to be strongly influenced by respiratory depth and rate [26]. Thus, while our study did not find significant changes in respiration between nausea levels (we asked subjects to try to maintain constant respiration), other studies found significant increases [10, 37] or decreases [21], which might have affected HRV results. Hence, interpretability of our results is improved and better supports the assertion that nausea is associated with decreased cardiovagal modulation and a sympathetic shift in sympathovagal balance.

We also applied a dynamic analysis approach to the HRV data, which utilized a previously validated point process algorithm to measure non-stationarities in HF over a much finer temporal window. This approach revealed phasic bursts of HF that accompanied transitions in nausea level. Bursts can be seen just prior to rating increases to “1”, “2”, and ”3.” These cardiovagal bursts may be associated with the autonomic “flushes” that can accompany nausea, and could then lead to interoceptive re-evaluation by the subject, culminating in the decision to rate a higher nausea intensity level. Such bursts may also be consistent with previous HRV studies for chemotherapy-induced nausea in patients, which demonstrated

that the standard deviation of successive differences (SDSD) metric, a proxy for cardiovagal modulation, peaked just prior to nausea onset [29]. In addition to these dynamic bursts, HF gradually decreased within a minute of nauseogenic stimulus initiation. Furthermore, within tens of seconds after nauseogenic stimulus cessation, HF gradually increased. This more gradual change may have reflected shifting anxiety levels in our subjects. Anxiety is known to influence both post-operative and chemotherapy-induced nausea [25, 35] and motion sickness [36]. In our study, anxiety likely increased as soon as the stimulus was presented (and before nausea was actually induced). Also, anxiety was likely diminished once the nauseogenic stimulus stopped, as subjects learned from the previous training session that cessation of stimulus would soon lead to the cessation of nausea sensation.

Skin conductance response increased both during nauseogenic stimulus presentation as well as with increasing nausea level, and continued increasing after cessation of stimulus. Other studies have found similar increases in skin conductance with increasing nausea stimulus duration [21]. Also, the persistence of elevated skin conduction into the post-stimulus period has been previously documented [10, 18]. Skin conductance is purely controlled by the sympathetic nervous outflow to sudomotor glands in the skin [5, 7, 17], and persistence of elevated skin conduction may have been due to the known long latency characterizing this autonomic outflow system [7]. Thus, our findings point to a highly persistent sympathetic outflow to the skin in response to nausea.

In contrast to skin conductance, which increased during nauseogenic stimulation and continued increasing after termination, we found that heart rate (HR) increased over the duration of stimulation and with increasing nausea level, only to drop off sharply after stimulus cessation. Increased HR is consistent with some studies which found HR increase in response to motion sickness [10, 21, 37], while other studies found no significant effect on heart rate [16, 30]. This seeming inconsistency may be due to differences in experimental and analysis procedures. Mullen et al. [30] averaged measurements over a very long period (15 minutes), during which subjects practiced random interval breathing, while Graybiel et al. [16] stopped stimulation periodically to take HR measurements, which may have affected the naturalistic context of progressively worsening motion sickness. For our study, the rapid decrease of heart rate immediately following nausea stimulus termination was also consistent with previous studies [10, 21]. As HR is influenced by both the sympathetic and parasympathetic branch of the ANS, our findings may have resulted from either an increase in cardio-sympathetic modulation or a decrease in cardio-vagal modulation.

Several limitations to our study should be noted. First, some subjects (5 out of 17) did not reach a nausea level 4 within the 20 minutes maximally allotted for stimulation. For consistency, these 5 subjects were not used for analyses involving the stimulus termination landmark only. However, these five subjects demonstrated similar results to the main group for other temporal landmarks so were likely not outliers and likely did not negatively skew the complete dataset. In addition, some subjects transitioned to higher nausea levels so quickly that there was minor overlap between test windows in our percept-related analysis. This happened for 2 (of 17) subjects, and a sub-analysis without these data did not change the final conclusions of our study. Another limitation was that our study population consisted entire of female subjects, due to limitations in recruitment. While gender appears to play only a minor role in motion sickness susceptibility [23], future studies should make a stronger effort to recruit male subjects. Finally, while a causal relationship is difficult to test with our approach, we have interpreted our findings to represent “nausea induced autonomic response,” as windows of interest in the percept analysis followed transitions in nausea level. However, as suggested by the dynamic HRV results, some autonomic responses (e.g. bursting HF increase) may actually precipitate and ultimately induce increased nausea perception. This complex phenomenon should be investigated in future studies.

In conclusion, we found increases in both skin conductance and heart rate in response to increasing levels of nausea. We also found decreased HF HRV and increased LF HRV, resulting in an increasing LF/HF ratio with increasing nausea. A recently developed dynamic HF HRV measure demonstrated that bursts of cardiovagal modulation may accompany (precede) transitions in percept level, as subjects become more nauseous. Our findings suggest a robust ANS response to increasing nausea perception, consistent with increased sympathetic and decreased parasympathetic modulation. Future studies should explore the neural correlates of this peripheral autonomic modulation.

Supplementary Material

Refer to Web version on PubMed Central for supplementary material.

Acknowledgments

We would like to thank NIH for funding support (RB: R01-HL084502; EB: R01-DA015644 and DP1-OD003646; VN: K01-AT002166, P01-AT002048, R01-AT004714; KP: F05-AT003770; BK: K23-DK069614), the NCRR (P41RR14075; CRC 1 UL1 RR025758-01), the Mental Illness and Neuroscience Discovery (MIND) Institute, and the International Foundation of Functional GI Disorders. Dr. Park was also supported by the Institute of Information Technology Advancement, Korea IITA-2008-(C1090-0801-0002). We would also like to thank Dr. Mark Vangel for technical assistance on statistical analyses of the data.

References

[1]. Anderson LA, Gross JB. Aromatherapy with peppermint, isopropyl alcohol, or placebo is equally effective in relieving postoperative nausea. J Perianesth Nurs. Feb; 2004 19(1):29–35. [PubMed: 14770380]

[2]. Barbieri R, Matten EC, Alabi AA, Brown EN. A point-process model of human heartbeat intervals: new definitions of heart rate and heart rate variability. Am J Physiol Heart Circ Physiol. Jan; 2005 288(1):H424–35. [PubMed: 15374824]

[3]. Barbieri R, Brown EN. Analysis of heartbeat dynamics by point process adaptive filtering. IEEE Trans Biomed Eng. Jan; 2006 53(1):4–12. [PubMed: 16402597]

[4]. Berntson GG, Bigger JT Jr. Eckberg DL, Grossman P, Kaufmann PG, Malik M, et al. Heart rate variability: origins, methods, and interpretive caveats. Psychophysiology. Nov; 1997 34(6):623–48. [PubMed: 9401419]

[5]. Bini G, Hagbarth KE, Hynninen P, Wallin BG. Thermoregulatory and rhythm-generating mechanisms governing the sudomotor and vasoconstrictor outflow in human cutaneous nerves. J Physiol. Sep.1980 306:537–52. [PubMed: 7463376]

[6]. Bos JE, Bles W. Motion sickness induced by optokinetic drums. Aviat Space Environ Med. Feb; 2004 75(2):172–4. [PubMed: 14960055]

[7]. Boucsein, W. Electrodermal Activity. Plenum Press; New York, NY: 1992.

[8]. Bubka A, Bonato F. Optokinetic drum tilt hastens the onset of vection-induced motion sickness. Aviat Space Environ Med. Apr; 2003 74(4):315–9. [PubMed: 12688448]

[9]. Cheung BS, Howard IP, Money KE. Visually-induced sickness in normal and bilaterally labyrinthinedefective subjects. Aviat Space Environ Med. Jun; 1991 62(6):527–31. [PubMed: 1859339]

[10]. Cowings PS, Suter S, Toscano WB, Kamiya J, Naifeh K. General autonomic components of motion sickness. Psychophysiology. Sep; 1986 23(5):542–51. [PubMed: 3809361]

[11]. Cowings PS, Naifeh KH, Toscano WB. The stability of individual patterns of autonomic responses to motion sickness stimulation. Aviat Space Environ Med. May; 1990 61(5):399–405. [PubMed: 2350308]

[12]. Denise P, Vouriot A, Normand H, Golding JF, Gresty MA. Effect of temporal relationship between respiration and body motion on motion sickness. Auton Neurosci. Dec 3; 2009 151(2): 142–6. [PubMed: 19592312]

[13]. Doweck I, Gordon CR, Shlitner A, Spitzer O, Gonen A, Binah O, et al. Alterations in R-R variability associated with experimental motion sickness. J Auton Nerv Syst. Dec 3; 1997 67(1–2):31–7. [PubMed: 9470142]

[14]. Goldberger AL, Amaral LA, Glass L, Hausdorff JM, Ivanov PC, Mark RG, et al. PhysioBank, PhysioToolkit, and PhysioNet: components of a new research resource for complex physiologic signals. Circulation. Jun 13; 2000 101(23):E215–20. [PubMed: 10851218]

[15]. Golding JF. Motion sickness susceptibility questionnaire revised and its relationship to other forms of sickness. Brain Res Bull. Nov 15; 1998 47(5):507–16. [PubMed: 10052582]

[16]. Graybiel A, Lackner JR. Evaluation of the relationship between motion sickness symptomatology and blood pressure, heart rate, and body temperature. Aviat Space Environ Med. Mar; 1980 51(3):211–4. [PubMed: 7362567]

[17]. Harm, DL. Motion sickness neurophysiology, physiological correlates, and treatment. In: Stanney, KM., editor. Handbook of Virtual Environments. Lawrence Erlbaum Associates; Mahwah, NJ: 2002. p. 637-61.

[18]. Isu N, Koo J, Takahashi N. Changes of skin potential level and of skin resistance level corresponding to lasting motion discomfort. Aviat Space Environ Med. Feb; 1987 58(2):136–42. [PubMed: 3827789]

[19]. Kennedy RS, Berbaum KS, Lilienthal MG, Smith MG. Disorientation and natural disequilibrium from simulated flight. International Symposium on Aviation Psychology. 1993; 7(26–29):799–804.

[20]. Kennedy RS, Drexler J, Kennedy RC. Research in visually induced motion sickness. Appl Ergon. Jul; 2010 41(4):494–503. [PubMed: 20170902]

[21]. Kim YY, Kim HJ, Kim EN, Ko HD, Kim HT. Characteristic changes in the physiological components of cybersickness. Psychophysiology. Sep; 2005 42(5):616–25. [PubMed: 16176385]

[22]. Klosterhalfen S, Kellermann S, Pan F, Stockhorst U, Hall G, Enck P. Effects of ethnicity and gender on motion sickness susceptibility. Aviat Space Environ Med. Nov; 2005 76(11):1051–7. [PubMed: 16313141]

[23]. Klosterhalfen S, Pan F, Kellermann S, Enck P. Gender and race as determinants of nausea induced by circular vection. Gend Med. Sep; 2006 3(3):236–42. [PubMed: 17081956]

[24]. Koch KL. Illusory self-motion and motion sickness: a model for brain-gut interactions and nausea. Dig Dis Sci. Aug; 1999 44(8 Suppl):53S–7S. [PubMed: 10490040]

[25]. Lee YY, Kim KH, Yom YH. Predictive models for post-operative nausea and vomiting in patients using patient-controlled analgesia. J Int Med Res. Jul–Aug; 2007 35(4):497–507. [PubMed: 17697527]

[26]. Malik M, Bigger JT Jr. Camm AJ, Kleiger RE, Malliani A, Moss AJ, et al. Heart rate variability. Standards of measurement, physiological interpretation, and clinical use. Task Force of the European Society of Cardiology and the North American Society of Pacing and Electrophysiology. Eur Heart J. Mar; 1996 17(3):354–81. [PubMed: 8737210]

[27]. Malik M, Camm A, Task Force of the European Society of Cardiology. Heart rate variability: standards of measurement, physiological interpretation and clinical use. Circulation. Mar 1; 1996 93(5):1043–65. [PubMed: 8598068]

[28]. Miller JC, Sharkey TJ, Graham GA, McCauley ME. Autonomic physiological data associated with simulator discomfort. Aviat Space Environ Med. Sep; 1993 64(9 Pt 1):813–9. [PubMed: 8216142]

[29]. Morrow GR, Andrews PL, Hickok JT, Stern R. Vagal changes following cancer chemotherapy: implications for the development of nausea. Psychophysiology. May; 2000 37(3):378–84. [PubMed: 10860415]

[30]. Mullen TJ, Berger RD, Oman CM, Cohen RJ. Human heart rate variability relation is unchanged during motion sickness. J Vestib Res. Jan–Feb; 1998 8(1):95–105. [PubMed: 9416595]

[31]. Muth ER. Motion and space sickness: intestinal and autonomic correlates. Auton Neurosci. Oct 30; 2006 129(1–2):58–66. [PubMed: 16950658]

[32]. Napadow V, Dhond R, Conti G, Makris N, Brown EN, Barbieri R. Brain correlates of autonomic modulation: combining heart rate variability with fMRI. Neuroimage. Aug 1; 2008 42(1):169–77. [PubMed: 18524629]

[33]. Oldfield RC. The assessment and analysis of handedness: the Edinburgh inventory. Neuropsychologia. Mar; 1971 9(1):97–113. [PubMed: 5146491]

[34]. Parker DE. The relative roles of the otolith organs and semicircular canals in producing space motion sickness. J Vestib Res. Jan–Feb; 1998 8(1):57–9. [PubMed: 9416590]

[35]. Shih V, Wan HS, Chan A. Clinical predictors of chemotherapy-induced nausea and vomiting in breast cancer patients receiving adjuvant doxorubicin and cyclophosphamide. Ann Pharmacother. Mar; 2009 43(3):444–52. [PubMed: 19193584]

[36]. Stern RM, Koch KL. Motion sickness and differential susceptibility. Curr Dir Psychol Sci. 1996; 5(4):115–20.

[37]. Stout CS, Toscano WB, Cowings PS. Reliability of psychophysiological responses across multiple motion sickness stimulation tests. J Vestib Res. Jan–Feb; 1995 5(1):25–33. [PubMed: 7711945]

[38]. Wiggins GC, Triantafyllou C, Potthast A, Reykowski A, Nittka M, Wald LL. 32-channel 3 Tesla receive only phased-array head coil with soccer-ball element geometry. Magn Reson Med. Jul; 2006 56(1):216–23. [PubMed: 16767762]

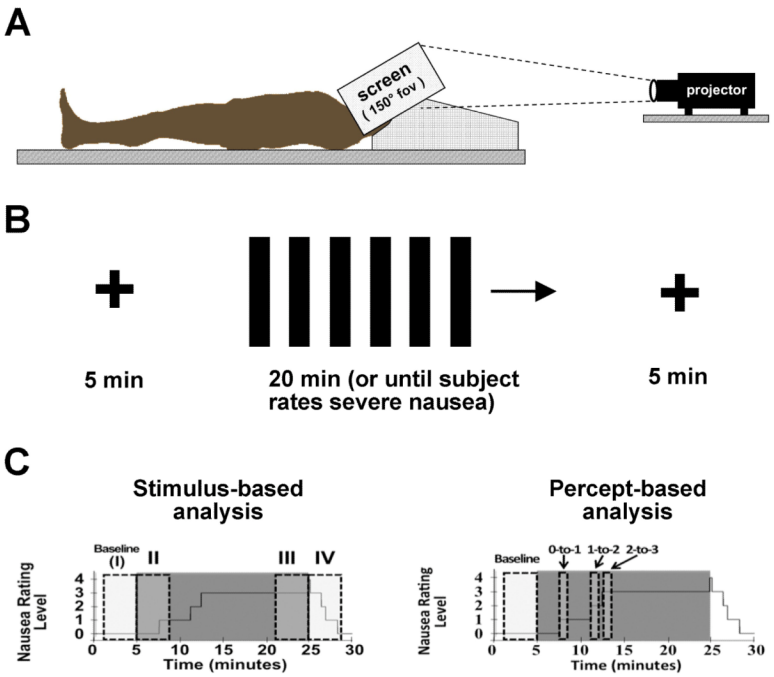

Figure 1.

Experimental procedure and analysis approach. (A) Subjects lay supine while a nauseogenic visual stimulation (horizontally translating stripes) was projected onto a full field-of-view screen from behind. (B) The visual stimulus was comprised by cross-hair fixation for 5 minutes before and after linear vection stimulus, which lasted up to 20minutes, or until the subjected rated a nausea level “4” for “severe” nausea. (C) Autonomic data were analyzed with both a stimulus-based (left) and percept-based (right) approach, where data averaged over discrete windows were compared to data collected during cross-hair fixation at baseline.

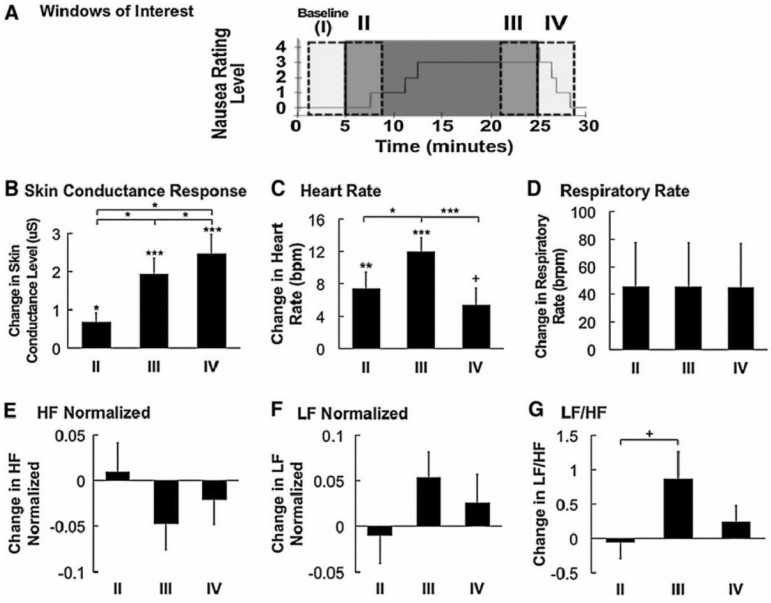

Figure 2.

Stimulus-based analysis of physiological indices. (A) Timing of 4-minute windows of interest are shown over a plot of a representative subject's nausea level. (B–G) Average change in skin conductance, HR, respiratory rate, normalized HF, normalized LF, and LF/HF ratio demonstrated significant increase in SCR and HR, and a trending increase in LF/HF ratio in response to increasing duration of nausea stimulus. While SCR remained elevated after cessation of nauseogenic stimulus, HR significantly decreased. Error bars indicate standard error of the mean. (+ 0.1>p>0.05,*0.05> p>0.01, **0.01>p>0.001, ***p<0.001).

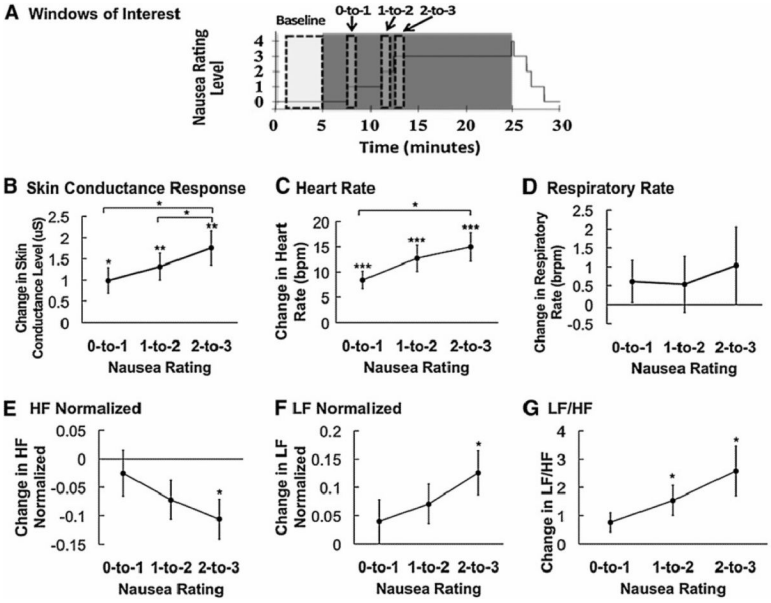

Figure 3.

Percept-based analysis of physiological indices. (A) Timing of 4-minute baseline and 1-minute post nausea rating transition windows are shown over a plot of a representative subject's nausea level. (B–G) Mean change in SCL, HR, respiratory rate, normalized HF, normalized LF, and LF/HF ratio reveal increases in SCL, HR, normalized LF, and LF/HF ratio with increasing nausea level. HF normalized decreased in response to increasing nausea level. Error bars indicate standard error of the mean. (+ 0.1>p>0.05,*0.05> p>0.01, **0.01>p>0.001, ***p<0.001).

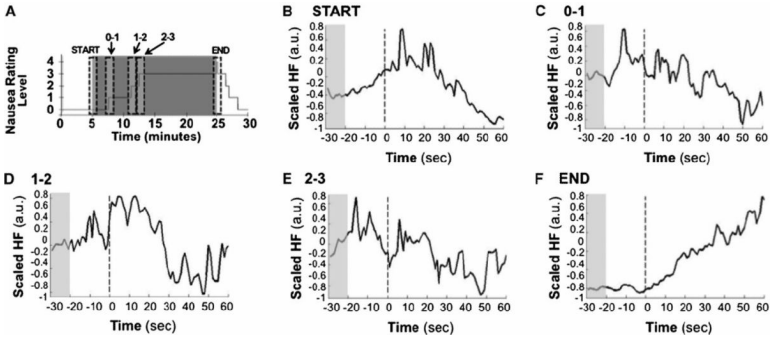

Figure 4.

Average across subjects of normalized point process HF HRV. (A) Schematic representation of the 90-second window placements. (B–F) HF HRV timeseries within windows of interest averaged across subjects demonstrate robust gradual decrease following stimulus initiation and gradual increase following stimulus cessation. Phasic bursts of HF power are noted prior to change in nausea perception.

Table 1

Skin Conductance Response. Difference from baseline for both stimulus-based and percept-based analyses.

Skin Conductance Response from Baseline		
Stimulus-Based Analysis		
II	***III***	***IV***
0.68 ± 0.98 μS (*)	1.94 ± 1.65 μS (***)	2.46 ± 2.11 μS (***)
Percept-Based Analysis		
"0-to-1"	***"1-to-2"***	***"2-to-3"***
0.99±1.26 μS (*)	1.32±1.31 μS (**)	1.76±1.68 μS (**)

+ 0.05<p<0.1

* 0.01<p<0.05

** 0.001<p<0.01

*** p<0.001

Table 2

Heart Rate. Difference from baseline for both stimulus-based and percept-based analyses.

Heart Rate Change from Baseline		
Stimulus-Based Analysis		
II	***III***	***IV***
7.4±8.2 bpm (**)	12.0±7.0 bpm (***)	5.4±8.1 bpm ($^{+}$)
Percept-Based Analysis		
"0-to-1"	***"1-to-2"***	***"2-to-3"***
8.4±7.0 bpm (***)	12.7±10.4 bpm (***)	15.0±11.4 bpm (***)

$^{+}$ $0.05<p<0.1$

* $0.01<p<0.05$

** $0.001<p<0.01$

*** $p<0.001$

Table 3

Heart Rate Variability. Difference from baseline for both stimulus-based and percept-based analyses.

Heart Rate Variability Change from Baseline (LF / HF Ratio)		
Stimulus-Based Analysis		
II	***III***	***IV***
−0.06±0.98 a.u. (n.s.)	0.87±1.57 a.u. (n.s.)	0.24±0.96 a.u. (n.s.)
Percept-Based Analysis		
"0-to-1"	***"1-to-2"***	***"2-to-3"***
0.76±1.36 a.u. (n.s.)	1.54±2.11 a.u. (*)	2.57±3.49 a.u. (*)

n.s. = not significant

+ 0.05<p<0.1

* 0.01<p<0.05

** 0.001<p<0.01

*** p<0.001